

LETTER TO THE EDITOR

The retrograde orbit of the HAT-P-6b exoplanet[★]

G. Hébrard^{1,2}, D. Ehrenreich³, F. Bouchy^{1,2}, X. Delfosse³, C. Moutou⁴, L. Arnold², I. Boisse^{5,1}, X. Bonfils³, R. F. Díaz^{1,2}, A. Eggenberger³, T. Forveille³, A.-M. Lagrange³, C. Lovis⁶, F. Pepe⁶, C. Perrier³, D. Queloz⁶, A. Santerne⁴, N. C. Santos^{5,7}, D. Ségransan⁶, S. Udry⁶, A. Vidal-Madjar¹

¹ Institut d'Astrophysique de Paris, UMR7095 CNRS, Université Pierre & Marie Curie, 98bis boulevard Arago, 75014 Paris, France
e-mail: hebrard@iap.fr

² Observatoire de Haute-Provence, CNRS/OAMP, 04870 Saint-Michel-l'Observatoire, France

³ UJF-Grenoble 1 / CNRS-INSU, Institut de Planétologie et d'Astrophysique de Grenoble (IPAG), UMR 5274, 38041 Grenoble, France

⁴ Laboratoire d'Astrophysique de Marseille, Univ. de Provence, CNRS (UMR6110), 38 r. F. Joliot Curie, 13388 Marseille cedex 13, France

⁵ Centro de Astrofísica, Universidade do Porto, Rua das Estrelas, 4150-762 Porto, Portugal

⁶ Observatoire de Genève, Université de Genève, 51 Chemin des Maillettes, 1290 Sauverny, Switzerland

⁷ Departamento de Física e Astronomia, Faculdade de Ciências, Universidade do Porto, Portugal

Received TBC; accepted TBC

ABSTRACT

We observed with the SOPHIE spectrograph (OHP, France) the transit of the HAT-P-6b exoplanet across its host star. The resulting stellar radial velocities display the Rossiter-McLaughlin anomaly and reveal a retrograde orbit: the planetary orbital spin and the stellar rotational spin point towards approximately opposite directions. A fit to the anomaly measures a sky-projected angle $\lambda = 166^\circ \pm 10^\circ$ between these two spin axes. All seven known retrograde planets are hot jupiters with masses $M_p < 3 M_{\text{Jup}}$. About two thirds of the planets in this mass range however are prograde and aligned ($\lambda \approx 0^\circ$). By contrast, most of the more massive planets ($M_p > 4 M_{\text{Jup}}$) are prograde but misaligned. Different mechanisms may therefore be responsible for planetary obliquities above and below $\sim 3.5 M_{\text{Jup}}$.

Key words. Planetary systems – Techniques: radial velocities – Stars: individual: HAT-P-6

1. Introduction

Spectroscopic observations during the transit of an exoplanet across its host star can measure the sky-projected angle between the spins of the planetary orbit and the stellar rotation (the obliquity) through the Rossiter-McLaughlin (RM) effect (Holt 1893; Rossiter 1924; McLaughlin 1924). The occultation of a rotating star by a planet distorts the apparent stellar line shape by removing the profile part emitted by the hidden portion of the star. This induces anomalous stellar radial velocity variations during the transit, which constrain the sky-projected obliquity (λ) and thus indicate whether the orbit is prograde, retrograde, or polar.

Queloz et al. (2000) reported the first detection of the RM anomaly for an extrasolar planet, HD 209458b. That planet shows an aligned, prograde orbit, as did all of the first seven planets for which the RM effect was measured (as reviewed in Hébrard et al. 2008). These early results were interpreted as a validation of theories of planetary formation and evolution where a single giant planet migrates in a proto-planetary disk perpendicular to the stellar spin axis (e.g. Lin et al. 1996). That migration is expected to conserve the initial alignment between the angular momentums of the disk and of the planetary orbits.

Hébrard et al. (2008) however found a first case of spin-orbit misalignment for the XO-3b planet, confirmed by Winn

et al. (2009a). Thereafter, Moutou et al. (2009) reported a second case, HD 80606 (see also Pont et al. 2009; Winn et al. 2009b; Hébrard et al. 2010). A dozen misaligned systems have now been identified, including some with retrograde or nearly polar orbits (e.g. Winn et al. 2009c; Narita et al. 2010a; Triaud et al. 2010; Simpson et al. 2010). These unexpected results favor alternative scenarios where close-in massive planets have been brought in by planet-planet (or planet-star) scattering, Kozai migration, and/or tidal friction (e.g. Malmberg et al. 2007; Fabrycky & Tremaine 2007; Chatterjee et al. 2008; Nagasawa et al. 2008; Guillochon et al. 2010). Alternatively, it has been proposed that the orbit still reflects the orientation of the disk, with the stellar spin instead having moved away, either early-on through magnetosphere-disk interactions (Lai et al. 2010), or later through elliptical tidal instability (Cébron et al. 2011). Distinguishing between these mechanisms needs additional obliquity measurements (e.g. Morton & Johnson 2010).

Here we present spectroscopic observations of one transit of HAT-P-6b. This hot jupiter transits a bright F star ($V = 10.5$) every 3.8 days and was discovered by Noyes et al. (2008, N08). Its mass is $1.06 \pm 0.12 M_{\text{Jup}}$ and its radius $1.33 \pm 0.06 R_{\text{Jup}}$.

2. Radial velocity measurements with SOPHIE

The August 21th 2010 transit of HAT-P-6b was observed with SOPHIE. This cross-dispersed, stabilized echelle spectrograph is dedicated to high-precision radial velocity measurements (Perruchot et al. 2008; Bouchy et al. 2009). It is fed by two optical fibers mounted at the focus of the 1.93-m telescope of the Haute-Provence Observatory (OHP, France). HAT-P-6 is bright

[★] Based on observations collected with the SOPHIE spectrograph on the 1.93-m telescope at Observatoire de Haute-Provence (CNRS), France, by the SOPHIE Consortium (program 10A.PNP.CON). SOPHIE radial velocities are available in electronic form at the CDS via anonymous ftp to cdsarc.u-strasbg.fr (130.79.128.5) or via http://cdsweb.u-strasbg.fr/cgi-bin/qcat?J/A+A/.

enough for observation in the high-resolution mode of the spectrograph ($\lambda/\Delta\lambda = 75,000$) and with fast detector readout.

The observations were carried out three days before full Moon. This was anticipated not to adversely impact the radial velocity accuracies, however, thanks to the large radial velocity shift between HAT-P-6 (-22.7 km s^{-1} , N08) and the Moon (close to the barycentric Earth radial velocity, which in the direction of HAT-P-6 was 16.3 km s^{-1} during the observations). We used the second fiber input to measure the sky background, and confirmed that its radial velocity was always shifted by at least 30 km s^{-1} from that of HAT-P-6. We therefore did not subtract the sky background as this would have introduced additional noise.

We collected 41 measurements during the transit night (JD $\approx 2\,455\,430.5$) between 20:10 and 03:40 UT. The sky was clear and the seeing stable around $1''.6$. The airmass first decreased from $\sec z = 1.8$ to 1.0 then increased to 1.1 at the end of the night. We adjusted the exposure times between 500 and 800 s to maintain a constant signal-to-noise ratio (SNR) of 39 per pixel at 550 nm. Spectra of a thorium lamp were obtained at the beginning and end of the 7.5-hour sequence, as well as three times during the sequence. These wavelength calibration exposures show that the spectrograph drifted by $\sim 2 \text{ m s}^{-1}$ per hour. We linearly interpolated between the calibration points to correct for this drift.

We used the SOPHIE pipeline (Bouchy et al. 2009) to extract the spectra, to cross-correlate them with a G2-type numerical mask, and to measure the radial velocities through Gaussian fits to the cross-correlation functions (CCFs) (Baranne et al. 1996; Pepe et al. 2002). We discarded the four bluest orders of the SOPHIE spectra that have low SNR; this slightly improves the dispersion of the data around the model. Every spectrum produces a clean CCF with a peak contrast of $11.45 \pm 0.10\%$ of the continuum and a full width at half maximum $\text{FWHM} = 12.61 \pm 0.08 \text{ km s}^{-1}$. The photon-noise uncertainty of the radial velocities, determined from the SNR of the spectra and the contrast and the FWHM of the CCF (see Boisse et al. 2010 for the details), is typically $\pm 18 \text{ m s}^{-1}$. It is quite large by SOPHIE standard because the star is early-type and a moderately fast rotator ($V \sin i_s = 8.0 \pm 1.0 \text{ km s}^{-1}$ and $T_{\text{eff}} = 6570 \pm 80 \text{ K}$; see below).

Figure 1 shows the SOPHIE velocities (see also the electronic table) as well as the orbital solution and HIRES data from N08. Outside transit, the SOPHIE data are compatible (within the expected arbitrary offset) with the HIRES orbit. During transit (lower panel), the SOPHIE data have obvious residuals relative to a Keplerian orbit, with a pattern opposite that expected for an aligned, prograde transit ($\lambda = 0^\circ$), red-shifted radial velocity in the first half of the transit followed by a symmetric blue shift. Here, the observed pattern of blue-shifts during the first part of the transit and red-shifts in the second part, instead, is characteristic of the RM anomaly with a retrograde orbit.

3. Analysis

We fit our SOPHIE data together with the HIRES data from N08 to determine the sky-projected obliquity in the HAT-P-6 system. Interestingly, two HIRES measurements were serendipitously obtained in transits, on December 16th, 2006 and July 4th, 2007 (the two squares in the lower panel of Fig. 1). They agree with the SOPHIE measurements secured at the same orbital phases and thus with a retrograde orbit.

The orbital elements of N08 determine the center of the August 21st 2010 transit, $T_{\text{tr}} = 2\,455\,430.4563 \pm 0.0018 \text{ BJD}$. This ± 2.6 -min uncertainty is negligible for our analysis. The 22 SOPHIE measurements secured outside transit determine the systemic, barycentric stellar velocity as $\gamma_{\text{SOPHIE}} = -22.594 \pm$

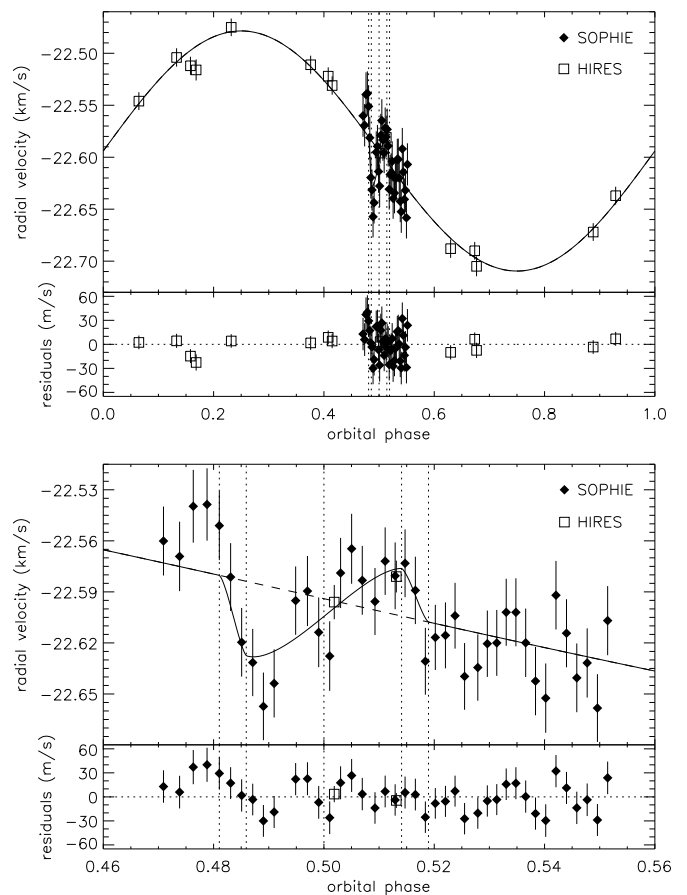


Fig. 1. Radial velocity measurements of HAT-P-6 as a function of orbital phase. Filled diamonds represent the SOPHIE data (this paper) and open squares the HIRES data (N08). The lower panel zooms on the transit phases. The dashed line represents the Keplerian fit (ignoring the transit phases) while the solid line represents the final fit including the model of the Rossiter-McLaughlin anomaly. In each panel, the residuals of the final fit are plotted below the data. The vertical dotted lines show the times of mid-transit, first, second, third, and fourth contacts. The fitted values are $V \sin i_s = 7.5 \pm 1.6 \text{ km s}^{-1}$ and $\lambda = 166^\circ \pm 10^\circ$.

0.007 km s^{-1} . The dispersion of their residuals from the orbital fit is 20.8 m s^{-1} . The error bars in the electronic table and Fig. 1 include an extra 9-m s^{-1} uncertainty added in quadrature to the photon noise to obtain a reduced χ^2 of 1. Similarly the 13 HIRES measurements outside transit determine a systemic velocity $\gamma_{\text{HIRES}} = -0.016 \pm 0.002 \text{ km s}^{-1}$ (HIRES velocities are relative) and have a 9.6-m s^{-1} dispersion around the Keplerian model. We quadratically added a 7.4-m s^{-1} jitter to their error bars (instead of the 8.6 m s^{-1} adopted by N08) to obtain a χ^2 of 1. The Ca II activity level measured from the SOPHIE spectra, $\log R'_{\text{HK}} = -5.03 \pm 0.10$, agrees reasonably with $\log R'_{\text{HK}} = -4.81$ measured by Wright (2005). It predicts a 10-m s^{-1} stellar jitter (Santos et al. 2000) consistent with these added dispersion terms.

We model the RM anomaly with the analytical first-moment approach developed by Ohta et al. (2005). We adopt the above values of the systemic velocities and mid-transit time, and the following parameters for the circular orbit taken from N08: ratio of the planetary and stellar radii $R_p/R_* = 0.09338 \pm 0.00053$, scaled semi-major axis $a/R_* = 7.69 \pm 0.22$, semi-amplitude of the radial velocity variation $K = 115.5 \pm 3.5 \text{ m s}^{-1}$, orbit inclination $i_o = 85:51 \pm 0:35$, and orbital period $P =$

3.852985 ± 0.000005 days. We compute from a model atmosphere (Kurucz 1979) a linear limb-darkening coefficient $\epsilon = 0.57 \pm 0.10$ in the 5300–6300 Å wavelength range.

The remaining two parameters of the Ohta et al. model are the sky-projected stellar rotational velocity $V \sin i_s$ and the sky-projected spin-orbit angle λ . We solve for these free parameters through a grid search, and derive formal confidence intervals from the χ^2 isocontours plotted in Fig. 2 (Hébrard et al. 2002). The resulting values are $V \sin i_s = 7.5 \pm 1.2 \text{ km s}^{-1}$ and $\lambda = 166^\circ \pm 6^\circ$. We separately propagate the effects of the uncertainties of the above fixed parameters on $V \sin i_s$ and λ , and find a $\pm 1.1 \text{ km s}^{-1}$ effect on $V \sin i_s$, dominated by the uncertainties on a/R_* , i , and γ_{SOPHIE} , and a $\pm 8^\circ$ effect on λ , mainly from the γ_{SOPHIE} uncertainty. The other fixed parameters contribute negligibly to the λ and $V \sin i_s$ uncertainties. Quadratic addition of the two sources of uncertainties produces our final results: $V \sin i_s = 7.5 \pm 1.6 \text{ km s}^{-1}$ and $\lambda = 166^\circ \pm 10^\circ$.

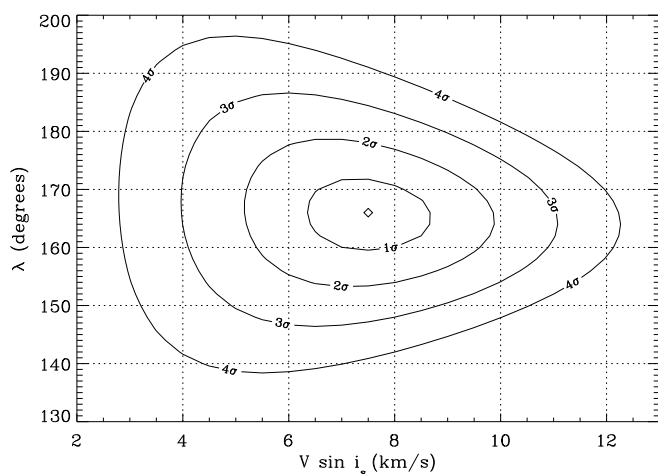


Fig. 2. χ^2 formal isocontours for our modeling of the Rossiter-McLaughlin effect as a function of λ and $V \sin i_s$ (see Sect. 3), using the formula from Ohta et al. (2005) and the system parameters from N08. The diamond shows the best values.

The resulting $V \sin i_s$ agrees with the $V \sin i_s = 8.0 \pm 1.0 \text{ km s}^{-1}$ which we derive from the width of the CCF of HAT-P-6 (Boisse et al. 2010), as well as with $V \sin i_s = 8.2 \pm 1.0 \text{ km s}^{-1}$ which N08 similarly derived from line broadening. The good agreement is somewhat surprising, since rotation broadens the lines of HAT-P-6 by significantly more than the SOPHIE resolution. As discussed by e.g. Hirano et al. (2010a) and Simpson et al. (2010), naive modeling of the RM anomaly could produce biased $V \sin i_s$ measurements under such circumstances.

Figure 1 plots the full dataset and the final fitted model. The SOPHIE and HIRES velocities have dispersions around this model of respectively 19.5 m s^{-1} and 9.0 m s^{-1} . These are similar to the dispersions of the radial velocities measured outside transit around the Keplerian model, 20.8 m s^{-1} and 9.6 m s^{-1} (see above). Our RM model is thus a good description of the measurements, with a reduced χ^2 of unity.

4. Discussion

The orbit of HAT-P-6b is retrograde with respect to the spin of its host star (Fig. 3), but the true, unprojected angle ψ between

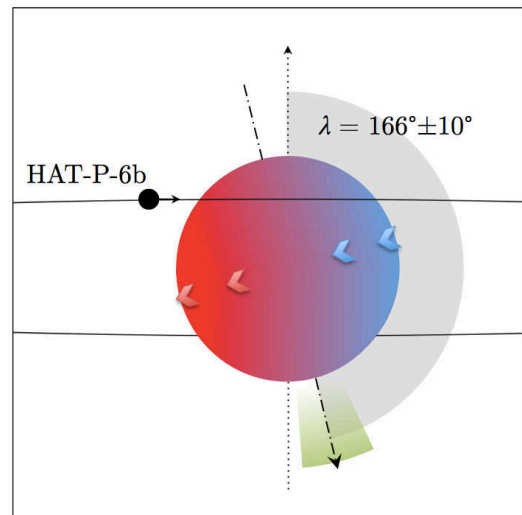


Fig. 3. Schematic view of the HAT-P-6 system from the Earth. The dotted and dashed-dotted lines represent the orbital angular momentum and the sky-projection of the stellar spin axis. The red and blue hues on the star surface indicate the Doppler shift from stellar rotation. The sky-projected obliquity λ and its uncertainty are displayed in grey and green.

the two angular momenta remains uncertain. We have only measured the *sky-projected* spin-orbit angle, $\lambda = 166^\circ \pm 10^\circ$, related to ψ by $\cos \psi = \sin i_s \cos \lambda \sin i_o + \cos i_s \cos i_o$ (e.g. Fabrycky & Winn 2009, whose notations and definitions we adopt: i_o is the inclination of the planetary orbit and i_s that of the stellar spin). The angle i_o is precisely known from the planetary transits but i_s remains unknown. The star cannot be *a priori* assumed to be seen edge-on ($i_s \simeq i_o \simeq 90^\circ$), especially here where $\lambda \neq 0$ demonstrates some misalignment. Comparisons of the measured $V \sin i_s$ to estimate the stellar rotation period P_{rot} and radius R_* can in principle constrain i_s , but here with ambiguous results.

On one hand, the measured R'_{HK} implies a short stellar rotation period, $P_{\text{rot}} \simeq 3.5$ days (Mamajek & Hillenbrand 2008). From $R_* = 1.46 \pm 0.06 R_\odot$ and $V \sin i_s = 8.0 \pm 1.0 \text{ km s}^{-1}$, we obtain $P_{\text{rot}} / \sin i_s = 9.2 \pm 1.5$ days. Reconciling the two numbers requires an almost pole-on star, with $i_s \simeq 20^\circ$ or 160° ¹, implying $\psi \simeq 110^\circ$. Schlaufman (2010), on the other hand, predicts $V_{\text{rot}} = 9.1 \text{ km s}^{-1}$ from the age and mass of HAT-P-6. This is similar to the measured $V \sin i_s$, so would instead imply a more edge-on star, with $i_s \simeq 60^\circ$ or 120° ², and $\psi \simeq 145^\circ$. Neither approach is expected to be accurate. Here they give inconsistent estimates for P_{rot} and therefore for i_s and ψ . Asteroseismology (Gizon & Solanki 2003), polarization of magnetic dipoles (López-Ariste et al. 2010), or accurate photometry may hopefully provide reliable i_s and P_{rot} measurements. In the mean time the value of ψ remains unknown, except for its being above 90° .

HAT-P-6b is the seventh planet identified as having a retrograde orbit, after WASP-2b, 8b, 15b and 17b (TriAUD et al. 2010; Queloz et al. 2010; Bayliss et al. 2010) and HAT-P-7b and 14b (Winn et al. 2009c, 2010a; Narita et al. 2009). Three planets additionally seem to have nearly polar orbits: CoRoT-1b (Pont et al. 2010), WASP-1b (Simpson et al. 2010), and HAT-P-11b (Winn et al. 2010b; Hirano 2010b). The last of those is also

¹ The $i_s \simeq 200^\circ$ and 340° formal solutions can be excluded since we know that the orbit is retrograde ($|\lambda| > \pi - i_o$).

² Here again, the retrograde orbit excludes $i_s \simeq 240^\circ$ and 300° .

likely retrograde. HAT-P-11b in addition is the only Neptune-mass planet with an obliquity measurement, with all other planetary systems with RM measurements being jovian mass planets.

The processes that produce tilted systems remain a matter of debate (see Sect. 1). Whether a single mechanism explains all close-in planets or whether different processes produce aligned and misaligned systems is unknown. Even whether the planetary orbits acquired obliquity or the stellar spin instead acquired tilt is uncertain. Those mechanisms, in any case, cannot require too narrowly specified conditions, since tilted systems are common.

Schlaufman (2010) and Winn et al. (2010c) hypothesized that misaligned planets preferentially orbit hot stars. The 6570 ± 80 K effective temperature of HAT-P-6 (N08) and the retrograde orbit of HAT-P-6b support this trend. As suggested by Johnson et al. (2009) and Hébrard et al. (2010), planetary mass apparently is also a key parameter. The seven retrograde and three polar planets all have masses below $3 M_{\text{Jup}}$. In that mass range, about a third of the planets with RM observations presents such extremes obliquities, with the other two thirds having $\lambda \simeq 0^\circ$.

Measured planets with masses above $4 M_{\text{Jup}}$ are fewer but they seem to have a different obliquity distribution: four (over six) of these massive planets are misaligned, but none with ultra-high obliquities, i.e. none on retrograde orbit and even none with $|\lambda| > 50^\circ$. Just two of the massive planets show $\lambda \simeq 0^\circ$, HAT-P-2b (Winn et al. 2007; Loeillet et al. 2008) and WASP-18 (Triaud et al. 2010). Curiously, the period distribution of exoplanets detected from radial velocity surveys changes at a similar characteristic mass. There is a distinct lack of planets with $M_p > 4 M_{\text{Jup}}$ in short-period orbits (< 100 days), and radial velocity surveys detect no planets above that limit outside multiple star systems (Udry et al. 2003; Boisse et al. 2010).

The changes in the λ -distribution with planetary mass is illustrated in Fig. 4 by the 37 systems with published λ and M_p . The inset zooms on the Jupiter-mass planets, with their 2/3 of aligned and 1/3 strongly misaligned planets. The massive planets, by contrast, mostly show significant but moderate misalignments. This suggests that distinct mechanisms dominate for different planet masses, with a critical mass near $3.5 M_{\text{Jup}}$. If a combination of planet scattering, Kozai mechanism, and tidal circularization explains most oblique, close-in planets (Nagasawa et al. 2008; Morton & Johnson 2010), planetary mass is a natural control parameter. These conclusions however currently suffer from small-number statistics. Additional Rossiter-McLaughlin observations of massive planets are needed to confirm that most of them are tilted and none of them are polar nor retrograde.

Acknowledgements. We thank the Haute-Provence Observatory staff who support the operation of SOPHIE. We acknowledge support of the “Programme National de Planétologie” (PNP) of CNRS/INSU, the Swiss National Science Foundation, and the French National Research Agency (ANR-08-JCJC-0102-01 and ANR-NT05-4-44463). D.E. is supported by CNES. A.E. is supported by a fellowship for advanced researchers from the Swiss National Science Foundation. I.B. and N.C.S. acknowledge the support by the European Research Council/European Community under the FP7 through Starting Grant agreement number 239953, as well as the support from Fundação para a Ciência e a Tecnologia (FCT) through program Ciência 2007 funded by FCT/MCTES (Portugal) and POPH/FSE (EC), and in the form of grants reference PTDC/CTE-AST/66643/2006 and PTDC/CTE-AST/098528/2008.

References

Baranne, A., Queloz, D., Mayor, M., et al. 1994, *A&AS*, 119, 373
 Bayliss, D., Winn, J., Mardling, R., Sackett, P. 2010, *ApJ*, 722, L224
 Boisse, I., Eggenberger, A., Santos, N. C., et al. 2010, *A&A*, 523, A88
 Bouchy, F., Hébrard, G., Udry, S., et al. 2009, *A&A*, 505, 853
 Cébron, D., Moutou, C., Le Bars, M., Le Gal, P., Fares, R. 2011 [arXiv:1101.4531]
 Chatterjee, S., Ford, E. B., Matsumura, S., Rasio, F. A. 2008, *ApJ*, 686, 580

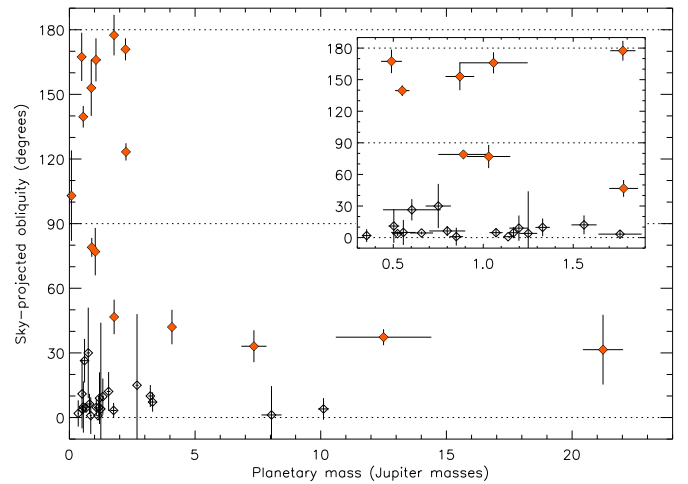


Fig. 4. Absolute value of λ , the sky-projected obliquity, as a function of planet mass M_p for the 37 planets with published RM measurements. In-filled, red markers denote systems with $|\lambda| > 30^\circ$. The inset zooms on $0.3 M_{\text{Jup}} < M_p < 1.9 M_{\text{Jup}}$. The dotted lines mark aligned-prograde, polar, and aligned-retrograde systems ($|\lambda| = 0^\circ, 90^\circ$, and 180° , respectively). The 37 plotted planetary systems are the 21 ones compiled in Hébrard et al. (2010), plus XO-4 (Narita et al. 2010a), WASP-1, 24, and 38 (Simpson et al. 2010), WASP-2, 4, 5, 15, and 18 (Triaud et al. 2010), WASP-8 (Queloz et al. 2010), WASP-19 (Hellier et al. 2011), HAT-P-4 and 14 (Winn et al. 2010a), HAT-P-8 (Simpson et al. 2010), HAT-P-11 (Winn et al. 2010b; Hirano 2010b), and HAT-P-6 (this work).

Fabrycky, D., Tremaine, S. 2007, *ApJ*, 669, 1298
 Fabrycky, D. C., Winn, J. N. 2009, *ApJ*, 696, 1230
 Gizon, L., Solanki, S. K. 2003, *ApJ*, 589, 1009
 Guillot, J., Ramirez-Ruiz, E., Lin, D. N. 2010, *ApJ*, sub. [arXiv:1012.2382]
 Hébrard, G., Lemoine, M., Vidal-Madjar, A., et al. 2002, *ApJ*, 140, 103
 Hébrard, G., Bouchy, F., Pont, F., et al. 2008, *A&A*, 481, 52
 Hébrard, G., Désert, J.-M., Díaz, R. F., et al. 2010, *A&A*, 516, A95
 Hellier, C., Anderson, D. R., Collier Cameron, A., et al. 2011 [arXiv:1009.5677]
 Hirano, T., Suto, Y., Taruya, A., et al. 2010a, *ApJ*, 709, 458
 Hirano, T., Narita, N., Shporer, A., et al. 2010b, *PASJ*, sub. [arXiv:1009.5677]
 Holt, J. R., 1893, *Astronomy and Astrophysics*, XII
 Johnson, J. A., Winn, J. N., Albrecht, S., et al. 2009, *PASP*, 121, 1104
 Kurucz, R. L. 1979, *ApJS*, 40, 1
 Lai, D., Foucart, F., Lin, D. N. C. 2010, *MNRAS*, in press [arXiv:1008.3148]
 Lin, D. N. C., Bodenheimer, P., Richardson, D. C. 1996, *Nature*, 380, 606
 Loeillet, B., Shporer, A., Bouchy, F., et al. 2008, *A&A*, 481, 529
 López-Ariste, A., et al. 2010, *A&A*, in press [arXiv:1011.6288]
 Malmberg, D., Davies, M. B., Chambers, J. E. 2007, *MNRAS*, 377, L1
 Mamajek, E. E., & Hillenbrand, L. A. 2008, *ApJ*, 687, 1264
 McLaughlin, D. B., 1924, *ApJ*, 60, 22
 Morton, T. D., Johnson, J. A. 2010, *ApJ*, in press [arXiv:1010.4025]
 Moutou, C., Hébrard, G., Bouchy, F., et al. 2009, *A&A*, 498, L5
 Nagasawa, M., Ida, S., Bessho, T. 2008, *ApJ*, 678, 498
 Narita, N., Sato, B., Hirano, T., Tamura, M. 2009, *PASJ*, 61, L35
 Narita, N., Hirano, T., Sanchis, R., et al. 2010a, *PASJ*, 62, L61
 Noyes, R. W., Bakos, G. À, Torres, G., et al. 2008, *ApJ*, 673, L79 (N08)
 Ohta, Y., Taruya, A., Suto, Y. 2005, *ApJ*, 622, 1118
 Pepe, F., Mayor, M., Galland, F., et al. 2002, *A&A*, 388, 632
 Perruchot, S., Kohler, D., Bouchy, F., et al. 2008, *SPIE proceedings*, 70140J
 Pont, F., Hébrard, G., Irwin, J. M., et al. 2009, *A&A*, 509, 695
 Pont, F., Endl, M., Cochran, W. D., et al. 2010, *MNRAS*, 402, L1
 Queloz, D., Eggenberger, A., Mayor, M., et al. 2000, *A&A*, 359, L13
 Queloz, D., Anderson, D., Collier Cameron, A., et al. 2010, *A&A*, 517, L1
 Rossiter, R. A., 1924, *ApJ*, 60, 15
 Santos, N. C., Mayor, M., Naef, D., et al. 2000, *A&A*, 361, 265
 Schlaufman, K. C. 2010, *ApJ*, 719, 602
 Simpson, E. K., et al. 2010, *MNRAS*, sub. [arXiv:1011.5664]
 Triaud, A., Collier Cameron, A., Queloz, D., et al. 2010, *A&A*, 524, A25
 Udry, S., Mayor, M., Santos, N. C. 2003, *A&A*, 407, 369

- Winn, J. N., Johnson, J. A., Peek, K. M. G., et al. 2007, *ApJ*, 665, L167
- Winn, J. N., Johnson, J. A., Fabrycky, D., et al. 2009a, *ApJ*, 700, 302
- Winn, J. N., Howard, A. W., Johnson, J. A., et al. 2009b, *ApJ*, 703, 2091
- Winn, J. N., Johnson, J. A., Albrecht, S., et al. 2009c, *ApJ*, 703, L99
- Winn, J. N., Howard, A., Johnson, J., et al. 2010a, *AJ*, 141, 63
- Winn, J. N., Johnson, J. A., Howard, A. W., et al. 2010b, *ApJ*, 723, L223
- Winn, J. N., Fabrycky, D., Albrecht, S., Johnson, J. A. 2010c, *ApJ*, 718, L145
- Wright, J. T. 2005, *PASP*, 117, 657